Journal of Magnetism and Magnetic Materials 517 (2021) 167215

Contents lists available at ScienceDirect

Journal of Magnetism and Magnetic Materials

journal homepage: www.elsevier.com/locate/jmmm

Research articles

Ferromagnetic resonance linewidth broadening induced by a tunable inhomogeneity effect

Yaowen Xing[a,b,1], Zhengren Yan[a,2], Jinwu Wei[a,c], Caihua Wan[a], Wenlong Yang[a], Yizhou Liu[a], Chi Fang[a], Xiao Wang[a], Chenyang Guo[a], Xiaomin Zhang[a], Guoqiang Yu[a,c], Xiufeng Han[a,b,c,*]

[a] Beijing National Laboratory for Condensed Matter Physics, Institute of Physics, University of Chinese Academy of Sciences, Chinese Academy of Sciences, Beijing 100190, China
[b] Center of Materials Science and Optoelectronics Engineering, University of Chinese Academy of Sciences, Beijing 100049, China
[c] Songshan Lake Materials Laboratory, Dongguan, Guangdong 523808, China

ARTICLE INFO

Keywords:
YIG
Linewidth broadening
Inhomogeneity effect
Dipolar interaction
Tunability

ABSTRACT

A phenomenon of $Y_3Fe_5O_{12}$ (YIG)-ferromagnetic-resonance (FMR) linewidth broadening in magnetically coupled YIG-Co films is reported. The broadened linewidth cannot be attributed to previous effects which only depend on the crystalline quality of YIG. Through micromagnetic simulation, the origin of this broadened linewidth was found to be a new type of inhomogeneity effect induced by the inhomogeneous dipolar field of Co layer. Furthermore, it shows that the extent of the linewidth broadening depends on the magnetization state of Co. The broadening is remarkable when the Co domains are random. The influence of Co on YIG-FMR linewidth still exists when the spacer between YIG and Co is 315 nm, indicating it is a long-range effect due to the dipolar origin.

1. Introduction

FMR linewidth is very important for both fundamental researches [1–9] and high frequency applications [10–13]. In general, for the magnetic films, the contributions to FMR linewidth include the intrinsic and extrinsic effects. The intrinsic effect is known as Gilbert damping, α, which originates from spin-orbit relaxation and magnon-phonon interaction [14–16]. In addition to the intrinsic Gilbert damping, three extrinsic effects can also contribute to the FMR linewidth in the previous references [5,8,9]. The first extrinsic effect is magnetic inhomogeneous broadening ΔH_0 due to sample imperfections [17]. ΔH_0 is always considered to be resonance-frequency-independent [17], for which it is also called zero-frequency offset [6]. The second extrinsic effect is two-magnon-scattering broadening ΔH_{2M}. It describes the process where the $k = 0$ magnon (FMR mode) is excited into $k \neq 0$ magnons (spin wave modes) [5,8] due to short-range defects [18]. The third extrinsic effect is mosaicity broadening ΔH_{mosaic} caused by long-range defects [8,18].

For a heterostructure consisting of two magnetic layers, its high frequency properties become more complex because they are influenced by the interactions between the two layers [19–34]. The interlayer interactions include: dipolar interaction [19], exchange interaction [20–28] and spin-currents-mediated interaction [29–34]. Therein, spin-current-mediated interaction describes the cases where spin currents are pumped from one magnetic layer into the other. The first magnetic layer where FMR happens acts as a source of spin currents due to spin pumping effect, while the second magnetic layer acts as a spin sink [32]. The influence of exchange interaction [21,24] and spin-current-mediated interaction [29–34] on FMR linewidth have been investigated. However, there are few systematic works for the influence of pure dipolar interaction on FMR linewidth in magnetically coupled heterostructures. In fact, the investigation of dipolar interaction is very fundamental because dipolar interaction exists in all these heterostructures.

In this work, we report the dipolar-interaction-mediated extrinsic linewidth broadening in YIG/MgO/Co/IrMn/Ru structures. The insulating MgO spacer is grown thick enough to exclude exchange interaction and spin-current-mediated interaction between YIG and Co. The only remaining interaction is of dipolar type. The influence of Co dipolar field on YIG-FMR is investigated in detail. We have found that

* Corresponding author at: Beijing National Laboratory for Condensed Matter Physics, Institute of Physics, University of Chinese Academy of Sciences, Chinese Academy of Sciences, Beijing 100190, China.
E-mail address: xfhan@iphy.ac.cn (X. Han).
[1] These two authors contributed equally to this work.
[2] These two authors contributed equally to this work.

https://doi.org/10.1016/j.jmmm.2020.167215
Received 4 February 2020; Received in revised form 3 July 2020; Accepted 3 July 2020
Available online 24 July 2020

the YIG-FMR intensity is strongly suppressed and the linewidth is strongly broadened during the magnetization switching of Co layer. Through micromagnetic simulation, the reason for this phenomenon is found to be an inhomogeneity effect induced by the inhomogeneous dipolar field of the Co layer.

2. Methods

We have fabricated six samples. The structure of Sample 1 is YIG (100 nm). Sample 2 is YIG(100)/MgO(15)/Co(3)/IrMn(10)/Ru(2 nm) (from bottom to top). Sample 3, 4, 5, 6 are YIG(100)/MgO(7.5)/Ru(d)/MgO(7.5)/Co(3)/IrMn(10)/Ru(2 nm) (d = 100, 200, 300, 500 nm). Firstly, YIG (100 nm) films were deposited on 500-μm $Gd_3Ga_5O_{12}$ (GGG) (111) substrates by an ultrahigh vacuum magnetron sputtering system (ULVACMPS-4000-HC7 model) with a base vacuum of 1×10^{-6} Pa. After deposition, high temperature annealing in air was carried out to further improve the crystalline quality of the YIG layers [35–37]. Then the surface of YIG was cleaned. Next, other layers were deposited on YIG (100 nm). During the deposition, a static magnetic field was applied to induce the unidirectional anisotropy axis of Co and exchange bias of IrMn.

The FMR experiments were measured by using the shorted microstrip line technique [38]. In this technique, the imaginary part of the permeability ($\mu = \mu' + i\mu''$) was obtained via measuring the complex S_{11} parameter of vector network analyzer (VNA). Then μ'' as a function of frequency was fitted by a Lorentz function and the resonance frequency f_r, intensity I and full width at half maximum (FWHM) Δf were extracted from this fitted Lorentz function. Finally, we got the magnetic field H dependence of f_r, I and Δf by sweeping H. It is worth noting that we used two sweep directions of H: one was increasing and the other was decreasing.

GPU-accelerated micromagnetic simulation framework (Mumax3) was used to calculate the FMR spectra of YIG [39]. In the simulation, the magnetic system is discretized into a mesh of dimensions 10 nm × 10 nm × 3 nm. The material-related parameters of YIG and Co are as follows. The saturation magnetization (M_s), the exchange stiffness constant (A) and the damping coefficient (α) are 1.39×10^5 A/m, 3.6×10^{-12} J/m and 0.001 for YIG, and 1.0×10^6 A/m, 1.5×10^{-11} J/m and 0.4 for Co, respectively. The size of simulated YIG layer is $2000\times 2000\times 99$ nm^3 and Co layer is $2000\times 2000\times 3$ nm^3 [40,41]. The thickness of the considered vacuum spacer between YIG and Co is 15 nm. The dipole-dipole interaction is considered. The FMR spectra are obtained with the help of Fourier transform of average magnetization of YIG under the Co dipolar field $\mathbf{H}_d$ and the applied field $\mathbf{H}_{app} = \mathbf{H}_s + \mathbf{H}_p$, where $\mathbf{H}_s$ is the statically uniform field along x axis and $\mathbf{H}_p$ is the pulsed magnetic field whose amplitude changes along the y axis [41].

The simulation steps are described in the following. The simulation begins with an initial random magnetic configuration which can be realized by Mumax3. Then the magnetization of Co (M_{Co}) layer relaxes to equilibrium under the given parameters including anisotropy field, exchange bias field and applied magnetic field. Subsequently, the random magnetic configuration of Co in different magnetization are obtained and the dipolar field induced by Co layer are calculated. Finally, we save the data of the dipolar field as one of the input parameter files of Mumax3 to further simulate the YIG-FMR peaks.

3. Results and discussions

Fig. 1(a) shows the structure of Sample 2. YIG is widely used in FMR experiments due to its ultralow Gilbert damping coefficient, α (10^{-5}–10^{-3}). The saturation magnetization of Co (M_s^{Co}) is much higher than that of YIG (M_s^{YIG}), which leads to the big difference in their FMR frequency. Therefore it is possible to independently investigate YIG-FMR with no regard to the Co-FMR in this experiment. MgO is insulating to exclude YIG-Co exchange interaction and 15 nm thickness is thick enough to exclude spin-current-mediated interaction [42,43]. IrMn is used to further separate the magnetization switching of YIG and Co, ensuring that the magnetization of YIG (M_{YIG}) remains unchanged while controlling M_{Co}. Ru is the cap layer for protecting IrMn from being oxidized. Fig. 1(b) shows M-H loops of Sample 1 (black) and Sample 2 (red). The magnetic field H was oriented in plane and parallel to the unidirectional anisotropy axis of Co. The black curves have been shifted vertically for comparison. For the red curves, the exchange bias field induced by IrMn is around 211 Oe. When $H \approx 211$ Oe, M_{Co} is antiparallel (parallel) to M_{YIG} as H increases (decreases). It is accessible to investigate YIG-FMR spectra difference between parallel (P) state and antiparallel (AP) state by choosing different sweep directions. We then measured FMR spectra of Sample 1 and 2 [Fig. 1(c, d)] with H increasing. The color represents the intensity of μ''. The V-shape red curves show YIG-FMR peaks at different values of H. For Sample 1, the FMR peaks become smaller (wider) in intensity (FWHM) as H increases (Fig. 1(e)). In contrast, for Sample 2, the FMR peaks first become smaller (wider) and then larger (narrower) in intensity (FWHM) (Fig. 1(f)). The minimum (maximum) of intensity (FWHM) occurs at 296 Oe, almost the same as the green dot ($M_{Co} = 0$) as indicated in Fig. 1(b). This coincidence indicates the influence of M_{Co} switching on the YIG-FMR in Sample 2.

We investigated in detail the H dependence of resonance frequency f_r, intensity I and FWHM Δf of YIG layer in Sample 1 and 2 as shown in Fig. 2(a)–(c) and (e)–(g), respectively. It is worth noting that the irrelevant points near zero field have been removed and the red (black) curves represent the data measured as H increases (decreases). For Sample 1, H dependence of resonance frequency f_r is shown in Fig. 2(a). I decreases continuously as $|H|$ increases [Fig. 2(b)], while Δf increases linearly as $|H|$ increases [Fig. 2(c)]. The red (black) curves are symmetric about $H = 0$ and there are almost no differences between increasing (red) and decreasing (black). For Sample 2, the case becomes different. In Fig. 2(e), when $H \approx 211$ Oe (exchange bias field of IrMn), the configuration of M_{YIG} and M_{Co} are AP (P) for the red (black) curves. YIG experiences different directions of Co dipolar field in these two states. The consistency of the red and black curves around 211 Oe indicates YIG-FMR resonance frequency f_r is barely influenced by the directions of Co dipolar field. The left (right) black dashed line is 126 Oe (296 Oe), representing the left (right) coercive field H_c^L (H_c^R) of Co as H decreases (increases), where $M_{Co} = 0$. The consistency of the red and black curves near the left (right) black dashed line indicates that the dipolar field of Co has almost no influence on YIG-FMR resonance frequency f_r when M_{Co} is switching.

However, the intensity I and FWHM Δf are remarkably affected [Fig. 2(f, g)]. I (Δf) is strongly suppressed (broadened) when M_{Co} is switching. As H increases (decreases), minimum I and maximum Δf occurs exactly at H_c^R (H_c^L). When M_{Co} is saturated by H, the phenomenon of intensity suppression and FWHM broadening disappears. For convenience, we use normalized magnetization $m_{Co} \equiv M_{Co}/M_s^{Co}$. As $|m_{Co}|$ becomes smaller, the suppression in I and broadening in Δf become stronger. YIG-FMR seems closely related to $|m_{Co}|$. Then the f_r dependence of linewidth ΔH is investigated as shown in Fig. 2(d, h) which are converted from Fig. 2(c, g) via Eq. (1):

$$\Delta H = \frac{\partial H}{\partial f_r} = \frac{2\pi}{\gamma}\frac{2}{\sqrt{4+\left(\frac{4\pi M_{eff}}{f_r}\frac{\gamma}{2\pi}\right)^2}} \quad (1)$$

Here $\gamma/2\pi$ and M_{eff} represent 2.8 MHz/Oe and effective magnetization of YIG, respectively. The intrinsic Gilbert damping coefficient, α, is related to the slope of ΔH-f_r curves due to Eq. (2) [1–4]:

$$\Delta H = \frac{2\pi}{\gamma}2\alpha f_r + \Delta H_0 \quad (2)$$

ΔH_0 is the broadening due to magnetic inhomogeneity [32]. Notably, Eq. (2) is only applicable to the linear ΔH-f_r curves such as the linear part of the red and black curves in Fig. 2(d, h). For the nonlinear part of the curves in Fig. 2(h), Eq. (2) turns inapplicable because of strong ΔH

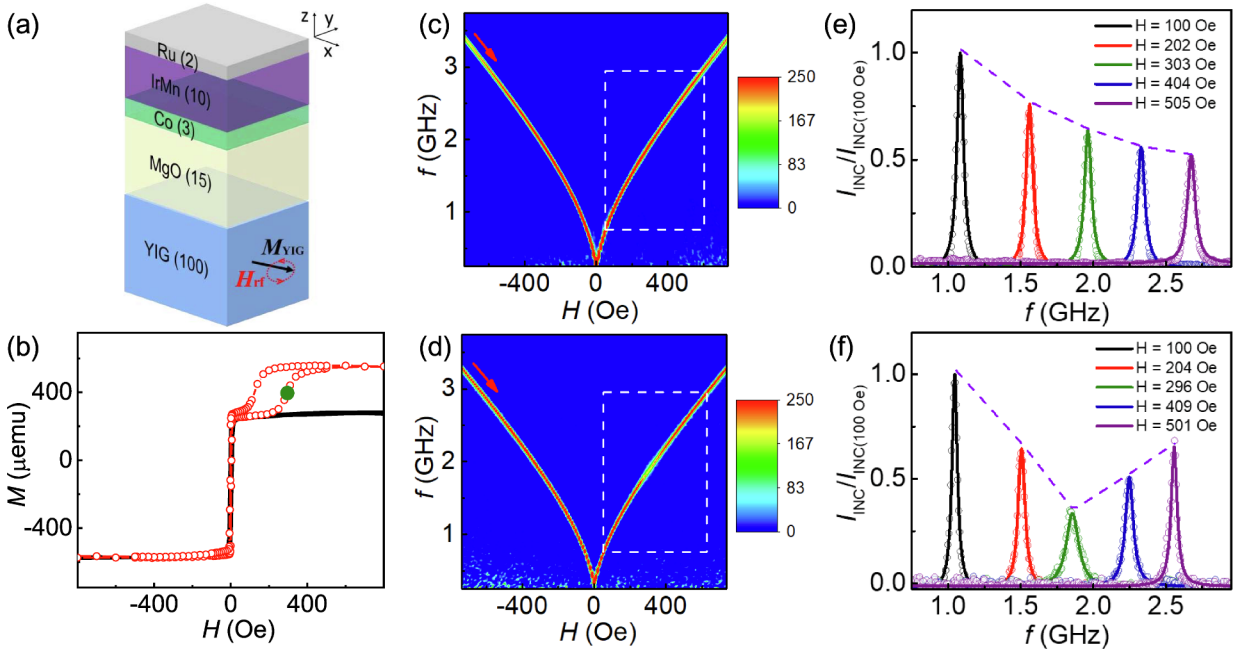

Fig. 1. Magnetic properties and YIG-FMR spectra of Sample 1 and 2. (a) Schematic diagram of the structure of Sample 2. (b) *M-H* loop of Sample 1 (black) and Sample 2 (red). The green dot represents $M_{Co} = 0$. (c) and (d) are FMR spectra of the YIG layer in Sample 1 and Sample 2, respectively. The red arrows represent that the sweep direction is increasing. The V-shape red curves represent the YIG-FMR peaks at different magnetic fields. (e) and (f) are the fitted Lorentz curves in five different fields extracted from the white dashed frames in (c) and (d), and all the intensity *I* has been normalized to $I_{INC(100\,Oe)}$ (The FMR intensity at $H = 100$ Oe as *H* increases). (For interpretation of the references to color in this figure legend, the reader is referred to the web version of this article.)

broadening correlated to m_{Co} changes.

All the previous inhomogeneity mechanisms, ΔH_0, ΔH_{2M} and ΔH_{mosaic}, cannot account for the linewidth broadening measured in our experiment due to the following reasons. ΔH_0 should have been independent on f_r. and ΔH_{mosaic} caused by short-range and long-range defects within the YIG layer [8,18] should have depended on the properties of YIG instead of $|m_{Co}|$. The above principles contradict our observations.

So we will assume that the YIG-FMR linewidth broadening in our experiment is caused by the inhomogeneous dipolar field of Co layer. As discussed above, the ΔH broadening depends on the value of $|m_{Co}|$. When $|m_{Co}| = 1$, there are almost no magnetic domains in the Co layer because M_{Co} is saturated by *H*. However, when $|m_{Co}| \neq 1$, the magnetic domains appear in the Co layer and their distribution is random. And when $|m_{Co}| = 0$, the distribution is most random. The random domains provide an inhomogeneous dipolar field on YIG, which introduces inhomogeneities in YIG. The inhomogeneities originating from Co are regarded as the key for the broadened ΔH. Eq. (3) taking the contribution of inhomogeneities into account can be expressed as below:

$$\Delta H = \frac{2\pi}{\gamma} 2\alpha f_r + \Delta H_0 + \Delta H_{Inho}^{dipole} \tag{3}$$

ΔH_{Inho}^{dipole} represents the contribution of the Co-dipolar-field-induced inhomogeneities in YIG. Micromagnetic simulation is used to verify this assumption. Fig. 3(a) shows the distribution of Co domains at H_c^R ($H = 296$ Oe, $m_{Co} = 0$). It is evident that the distribution is random. The sizes of Co domains are mainly tens or hundreds of nanometers. The area of Co layer in Sample 2 is 5 mm × 10 mm, hence there are about

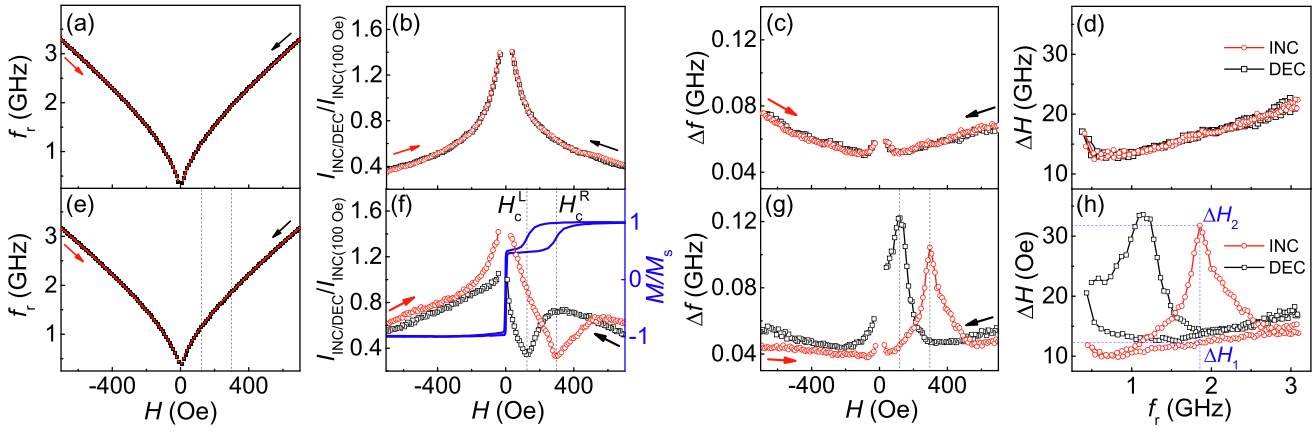

Fig. 2. YIG-FMR properties of Sample 1 and 2. (a)–(c) and (e)–(g) are *H* dependence of resonance frequency f_r, intensity *I* and FWHM Δf of Sample 1 and 2, respectively. (d) and (h) are the f_r dependence of ΔH converted from (c) and (g). Black (red) curves represent that the sweep direction is decreasing (increasing) in (a)–(h). The left (right) black dashed lines in (e)–(g) represent the field where $M_{Co} = 0$ as *H* decreases (increases). In (b) and (f), all the intensity *I* has been normalized to $I_{INC(100\,Oe)}$. In (f), the blue curves represent M/M_s-*H* loop of Sample 2. (For interpretation of the references to color in this figure legend, the reader is referred to the web version of this article.)

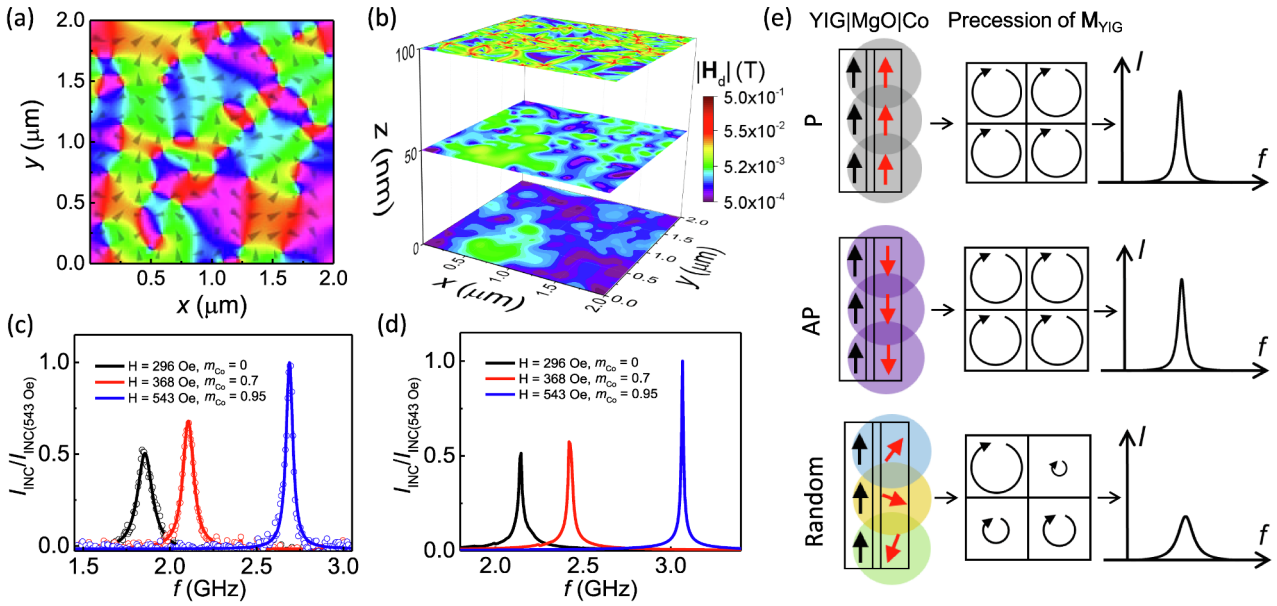

Fig. 3. Micromagnetic simulation results. (a) Randomly distributed magnetic domains in the Co layer at $m_{Co} = 0$. The gray arrows show the orientation of the in-plane magnetization. (b) Distribution of the magnitude of the Co-induced dipolar field ($|\mathbf{H}_d|$) in 100 nm YIG layer at different depths. Measured FMR peaks (c) and simulated peaks (d) with different applied fields (H) and magnetization states of Co (m_{Co}). Black, red, and blue peaks represent $H = 296$ Oe ($m_{Co} = 0$), $H = 368$ Oe ($m_{Co} = 0.7$) and $H = 543$ Oe ($m_{Co} = 0.95$). In (c) and (d), all the intensity I has been normalized to $I_{INC(543\,Oe)}$. (e) The schematic diagram of the inhomogeneity effect. (For interpretation of the references to color in this figure legend, the reader is referred to the web version of this article.)

10^4–10^6 domains when $m_{Co} = 0$. Fig. 3(b) shows the distribution of the magnitude of the dipolar field ($|\mathbf{H}_d|$) in 100 nm YIG at different depths induced by the random Co domains when $m_{Co} = 0$. Obviously, M_{YIG} in different regions experiences diverse dipolar fields, which leads to great inhomogeneities in the YIG layer. Fig. 3(c) shows YIG-FMR peaks of Sample 2 at $H = 296$ Oe, 368 Oe and 543 Oe. The peaks become higher and narrower as H increases. This trend is different from Sample 1. Fig. 3(d) shows the simulation results at the same fields, consistent well with the experiment. In this micromagnetic simulation, we have considered the influence from the inhomogeneous dipolar field of Co on YIG-FMR. The consistency strongly supports our assumption. When $H = 296$ Oe ($m_{Co} = 0$), the randomness of Co domains is maximum. It results in the greatest inhomogeneities inside YIG. Hence, YIG-FMR peak has the smallest I and widest Δf in this case. When $H = 368$ Oe ($m_{Co} = 0.7$) and $H = 543$ Oe ($m_{Co} = 0.95$), randomness of the Co domains decreases, thus the YIG-FMR peaks become higher and narrower.

The detail of this new inhomogeneity effect should be further explained. Fig. 3(e) shows the influential mechanism of the inhomogeneous Co dipolar field on YIG-FMR. When M_{Co} is saturated by H, whether P or AP to M_{YIG}, Co domains disappear. The dipolar field of Co is homogeneous in this case. M_{YIG} in different regions experiences almost the same dipolar field and precesses in almost the same frequency when YIG-FMR occurs. Therefore the FMR peak is high in intensity and narrow in FWHM. In contrast, when M_{Co} is switching, a number of Co domains appear and M_{Co} of these domains possesses different magnitudes and directions. The random states of Co domains induce an inhomogeneous distribution of dipolar field around Co layer. M_{YIG} in different regions experiences diverse dipolar fields and precesses in different frequencies and amplitudes, which results in the splits of the resonance frequency f_r. Thus the FMR peak is small and wide in this case. Looking back on previous inhomogeneity effects: sample-imperfections-induced ΔH_0, short-range-defects-induced ΔH_{2M} and long-range-defects-induced ΔH_{mosaic}, ΔH_{Inho}^{dipole} can also be regarded as a kind of dipolar-field-imperfections-induced linewidth broadening. The imperfect dipolar field can be large as 0.5T as seen in Fig. 3(b), hence the inhomogeneity effect is remarkable. Moreover, this inhomogeneity effect points to a relationship between I and Δf (ΔH). When I is suppressed, Δf (ΔH) is broadened at the same time due to the same physical origin.

Higher intensity and narrower linewidth are expected in fundamental researches and high frequency applications. Higher intensity is beneficial to detect high frequency signals in FMR and spin waves experiments [44,45], whereas a narrower linewidth improves the quality factors of the high frequency resonator [10,12,13]. However, when the reseachers investigate the systems consisting of two or more magnetic layers, the dipolar-interaction-induced inhomogeneity effect should be considered. For obtaining higher intensity and narrower linewidth, the reseachers should try to avoid the inhomogeneity effect, which may not get enough attention in the previous researches.

It is worth noting that the magnetic field and frequency range where the linewidth broadening is observed can be modified by changing the thickness of the Co layer. For the case that the thickness of Co $t_{Co} = 3$ nm, we define a parameter called *tunability* to characterize the ratio of maximum broadening in linewidth by Eq. (4):

$$Tunability = \frac{\Delta H_2 - \Delta H_1}{\Delta H_1} \times 100\% \tag{4}$$

ΔH_1 and ΔH_2 are shown in Fig. 2(h). ΔH_2 represents the linewidth at $m_{Co} = 0$ ($H > 0$), while ΔH_1 represents the linewidth at the same frequency ($H < 0$). Fig. 4 shows YIG-Co non-magnetic spacer thickness dependence of *tunability*. During the FMR measurements for Samples 2 to 6, the magnetic field H was oriented in plane and parallel to the unidirectional anisotropy axis of Co. When the spacer between YIG and Co is 15 nm, *tunability* = 158%. When the spacer increases to 115 nm, *tunability* = 152%, indicating a tiny decrease of the inhomogeneity effect. The inhomogeneity effect still works when the spacer increases to 315 nm (*tunability* = 33%). Finally, when the spacer increases to 515 nm, *tunability* = 0% below detection sensitivity. The thickness-dependence investigation indicates the inhomogeneity effect to be a long-range effect caused by the dipolar interaction.

4. Conclusion

In conclusion, we have fabricated YIG(100)/MgO(15)/Co(3)/IrMn

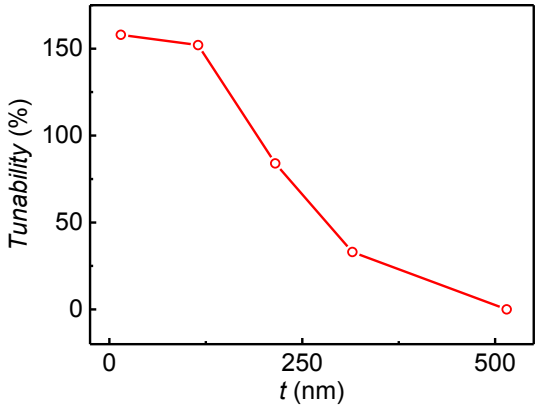

Fig. 4. YIG-Co non-magnetic spacer thickness dependence of *tunability*. t represents the total thickness of MgO(7.5)/Ru(d)/MgO(7.5), namely, $t = d + 15$.

(10)/Ru(2 nm) and

YIG(100)/MgO(7.5)/Ru(d)/MgO(7.5)/Co(3)/IrMn(10)/Ru(2 nm) (d = 100, 200, 300, 500 nm) structures. In these structures (except Sample 6), the YIG-FMR intensity I is suppressed and the linewidth ΔH is broadened when M_{Co} is switching. The reason is found to be the inhomogeneity effect through micromagnetic simulation. Moreover, the thickness dependence of *tunability* results shows that the inhomogeneity effect is such a long-range effect, which is over 315 nm. Our experiment results reveal that the influence of the dipolar interaction on FMR is remarkable in magnetically coupled heterostructures. Researchers should pay more attention to the dipolar interaction while investigating these systems.

CRediT authorship contribution statement

Yaowen Xing: Investigation, Writing - original draft, Writing - review & editing. **Zhengren Yan:** Software, Formal analysis, Writing - review & editing. **Jinwu Wei:** Methodology, Writing - review & editing. **Caihua Wan:** Conceptualization, Writing - review & editing. **Wenlong Yang:** Conceptualization, Resources. **Yizhou Liu:** Software, Formal analysis. **Chi Fang:** Methodology, Resources. **Xiao Wang:** Resources, Writing - review & editing. **Chenyang Guo:** Conceptualization, Writing - review & editing. **Xiaomin Zhang:** Resources, Writing - review & editing. **Guoqiang Yu:** Conceptualization, Supervision. **Xiufeng Han:** Writing - review & editing, Supervision, Project administration.

Declaration of Competing Interest

The authors declare that they have no known competing financial interests or personal relationships that could have appeared to influence the work reported in this paper.

Acknowledgements

This work was supported by the National Key Research and Development Program of China [MOST, Grants No. 2017YFA0206200 and 2016YFA0300802], the National Natural Science Foundation of China [NSFC, Grants No. 51831012, No. 11974398 and No. 51620105004] and partially supported by the Strategic Priority Research Program (B) [Grant No. XDB07030200], the International Partnership Program (Grant No.112111KYSB20170090), the Key Research Program of Frontier Sciences (Grant No. QYZDJ-SSWSLH016) and CAS-ITRI bilateral cooperation project (CAS-ITRI201907) of the Chinese Academy of Sciences (CAS).

Appendix A. Supplementary data

Supplementary data associated with this article can be found, in the online version, at https://doi.org/10.1016/j.jmmm.2020.167215.

References

[1] T.D. Rossing, Resonance linewidth and anisotropy variation in thin films, J. Appl. Phys. 34 (4) (1963), https://doi.org/10.1063/1.1729582 995–995.
[2] S.S. Kalarickal, P. Krivosik, M. Wu, C.E. Patton, M.L. Schneider, P. Kabos, T.J. Silva, J.P. Nibarger, Ferromagnetic resonance linewidth in metallic thin films: Comparison of measurement methods, J. Appl. Phys. 99 (9) (2006) 093909, , https://doi.org/10.1063/1.2197087.
[3] J.M. Shaw, T.J. Silva, M.L. Schneider, R.D. McMichael, Spin dynamics and mode structure in nanomagnet arrays: Effects of size and thickness on linewidth and damping, Phys. Rev. B 79 (18) (2009) 184404, https://doi.org/10.1103/PhysRevB.79.184404.
[4] J.M. Shaw, H.T. Nembach, T.J. Silva, Determination of spin pumping as a source of linewidth in sputtered $Co_{90}Fe_{10}$/Pd multilayers by use of broadband ferromagnetic resonance spectroscopy, Phys. Rev. B 85 (5) (2012) 054412, , https://doi.org/10.1103/PhysRevB.85.054412.
[5] L. Chen, S. Mankovsky, S. Wimmer, M.A.W. Schoen, H.S. Körner, M. Kronseder, D. Schuh, D. Bougeard, H. Ebert, D. Weiss, C.H. Back, Emergence of anisotropic Gilbert damping in ultrathin Fe layers on GaAs(001), Nat. Phys. 14 (5) (2018) 490–494, https://doi.org/10.1038/s41567-018-0053-8.
[6] Z. Celinski, B. Heinrich, Ferromagnetic resonance linewidth of Fe ultrathin films grown on a bcc Cu substrate, J. Appl. Phys. 70 (10) (1991) 5935–5937, https://doi.org/10.1063/1.350110.
[7] B. Heinrich, J.F. Cochran, R. Hasegawa, FMR linebroadening in metals due to two-magnon scattering, J. Appl. Phys. 57 (8) (1985) 3690–3692, https://doi.org/10.1063/1.334991.
[8] K. Zakeri, J. Lindner, I. Barsukov, R. Meckenstock, M. Farle, U. von Hörsten, H. Wende, W. Keune, J. Rocker, S.S. Kalarickal, K. Lenz, W. Kuch, K. Baberschke, Z. Frait, Spin dynamics in ferromagnets: Gilbert damping and two-magnon scattering, Phys. Rev. B 76 (10) (2007) 104416, https://doi.org/10.1103/PhysRevB.76.104416.
[9] H. Sakimura, A. Asami, H. Hayashi, T. Harumoto, Y. Nakamura, J. Shi, K. Ando, Intrinsic spin decay length in an antiferromagnetic insulator, Phys. Rev. Res. 1 (1) (2019) 013013, , https://doi.org/10.1103/PhysRevResearch.1.013013.
[10] B.K. Kuanr, D.L. Marvin, T.M. Christensen, R.E. Camley, Z. Celinski, High-frequency magnetic microstrip local bandpass filters, Appl. Phys. Lett. 87 (22) (2005) 222506, https://doi.org/10.1063/1.2138364.
[11] B. Kuanr, Z. Celinski, R.E. Camley, Tunable high-frequency band-stop magnetic filters, Appl. Phys. Lett. 83 (19) (2003) 3969–3971, https://doi.org/10.1063/1.1625424.
[12] A.B. Ustinov, B.A. Kalinikos, V.S. Tiberkevich, A.N. Slavin, G. Srinivasan, Q factor of dual-tunable microwave resonators based on yttrium iron garnet and barium strontium titanate layered structures, J. Appl. Phys. 103 (6) (2008) 063908, https://doi.org/10.1063/1.2895006.
[13] L.F. Chen, C.K. Ong, C.P. Neo, V.V. Varadan, V.K. Varadan, Microwave Theory and Techniques for Materials Characterization, John Wiley and Sons Ltd (2004) 37–141, https://doi.org/10.1002/0470020466.ch2.
[14] B. Heinrich, Spin Relaxation in Magnetic Metallic Layers and Multilayers, Springer-Verlag, Berlin, Heidelberg, 2005, pp. 143–210, https://doi.org/10.1007/3-540-27163-5_5 .
[15] C.K.A. Mewes, T. Mewes, Relaxation in Magnetic Materials for Spintronics, Pan Stanford (2015) 71–95 URL: https://www.taylorfrancis.com/books/e/9780429069215/chapters/10.1201.
[16] B. Khodadadi, A. Rai, A. Sapkota, A. Srivastava, B. Nepal, Lim, Conductivity-Like Gilbert Damping due to Intraband Scattering in Epitaxial Iron, arXiv e-prints (2019). https://arxiv.xilesou.top/abs/1906.10326.
[17] W. Platow, A.N. Anisimov, G.L. Dunifer, M. Farle, K. Baberschke, Correlations between ferromagnetic-resonance linewidths and sample quality in the study of metallic ultrathin films, Phys. Rev. B 58 (9) (1998) 5611–5621, https://doi.org/10.1103/PhysRevB.58.5611.
[18] R.D. McMichael, D.J. Twisselmann, A. Kunz, Localized ferromagnetic resonance in inhomogeneous thin films, Phys. Rev. Lett. 90 (22) (2003) 227601, https://doi.org/10.1103/PhysRevLett.90.227601 https://link.aps.org/doi/10.1103/PhysRevLett.90.227601.
[19] D. Markó, F. Valdés-Bango, C. Quirós, A. Hierro-Rodríguez, M. Vélez, J.I. Martín, J.M. Alameda, D.S. Schmool, L.M. Álvarez-Prado, Tunable ferromagnetic resonance in coupled trilayers with crossed in-plane and perpendicular magnetic anisotropies, Appl. Phys. Lett. 115 (8) (2019) 082401, https://doi.org/10.1063/1.5104341.
[20] J.J. Krebs, P. Lubitz, A. Chaiken, G.A. Prinz, Magnetic resonance determination of the antiferromagnetic coupling of Fe layers through Cr, Phys. Rev. Lett. 63 (15) (1989) 1645–1648, https://doi.org/10.1103/PhysRevLett.63.1645 https://link.aps.org/doi/10.1103/PhysRevLett.63.1645.
[21] A. Layadi, J.O. Artman, Ferromagnetic resonance in a coupled two-layer system, J. Magn. Magn. Mater. 92 (1) (1990) 143–154, https://doi.org/10.1016/0304-8853(90)90691-I URL: http://www.sciencedirect.com/science/article/pii/030488539090691I.
[22] J. Lindner, K. Baberschke, In situferromagnetic resonance: an ultimate tool to investigate the coupling in ultrathin magnetic films, J. Phys. Condens. Matter 15 (4) (2003) R193–R232, https://doi.org/10.1088/0953-8984/15/4/204.

[23] J.J. Krebs, P. Lubitz, A. Chaiken, G.A. Prinz, Observation of magnetic resonance modes of Fe layers coupled via intervening Cr (invited), J. Appl. Phys. 67 (9) (1990) 5920–5924, https://doi.org/10.1063/1.346015.
[24] A. Layadi, J.O. Artman, Study of antiferromagnetic coupling by ferromagnetic resonance (FMR), J. Magn. Magn. Mater. 176 (2) (1997) 175–182, https://doi.org/10.1016/S0304-8853(97)00142-X URL: http://www.sciencedirect.com/science/article/pii/S030488539700142X.
[25] J. Lindner, K. Baberschke, Ferromagnetic resonance in coupled ultrathin films, J. Phys. Condens. Matter 15 (5) (2003) S465–S478, https://doi.org/10.1088/0953-8984/15/5/303.
[26] C. Vittoria, Ferromagnetic resonance of exchange-coupled magnetic layers, Phys. Rev. B 37 (4) (1988) 2387–2390, https://doi.org/10.1103/PhysRevB.37.2387 https://link.aps.org/doi/10.1103/PhysRevB.37.2387.
[27] S. Klingler, V. Amin, S. Geprägs, K. Ganzhorn, H. Maier-Flaig, M. Althammer, H. Huebl, R. Gross, R.D. McMichael, M.D. Stiles, S.T.B. Goennenwein, M. Weiler, Spin-torque excitation of perpendicular standing spin waves in coupled YIG/Co heterostructures, Phys. Rev. Lett. 120 (12) (2018) 127201, https://doi.org/10.1103/PhysRevLett.120.127201 https://link.aps.org/doi/10.1103/PhysRevLett.120.127201.
[28] H. Qin, S.J. Hämäläinen, S. van Dijken, Exchange-torque-induced excitation of perpendicular standing spin waves in nanometer-thick YIG films, Sci. Rep. 8 (1) (2018) 5755, https://doi.org/10.1038/s41598-018-23933-y.
[29] B. Heinrich, Y. Tserkovnyak, G. Woltersdorf, A. Brataas, R. Urban, G.E.W. Bauer, Dynamic exchange coupling in magnetic bilayers, Phys. Rev. Lett. 90 (18) (2003) 187601, , https://doi.org/10.1103/PhysRevLett.90.187601 https://link.aps.org/doi/10.1103/PhysRevLett.90.187601.
[30] E. Popova, C. Tiusan, A. Schuhl, F. Gendron, N.A. Lesnik, Ferromagnetic resonance in the epitaxial system Fe/MgO/Fe with coupled magnetic layers, Phys. Rev. B 74 (22) (2006) 224415, https://doi.org/10.1103/PhysRevB.74.224415 https://link.aps.org/doi/10.1103/PhysRevB.74.224415.
[31] B. Heinrich, G. Woltersdorf, R. Urban, E. Simanek, Role of dynamic exchange coupling in magnetic relaxations of metallic multilayer films (invited), J. Appl. Phys. 93 (10) (2003) 7545–7550, https://doi.org/10.1063/1.1543852.
[32] B. Heinrich, C. Burrowes, E. Montoya, B. Kardasz, E. Girt, Y.-Y. Song, Y. Sun, M. Wu, Spin pumping at the magnetic insulator (YIG)/normal metal (Au) interfaces, Phys. Rev. Lett. 107 (6) (2011) 066604, https://doi.org/10.1103/PhysRevLett.107.066604 https://link.aps.org/doi/10.1103/PhysRevLett.107.066604.
[33] A. Kamra, D.M. Polishchuk, V. Korenivski, A. Brataas, Anisotropic and controllable Gilbert-Bloch dissipation in spin valves, Phys. Rev. Lett. 122 (14) (2019) 147201, https://doi.org/10.1103/PhysRevLett.122.147201 https://link.aps.org/doi/10.1103/PhysRevLett.122.147201.
[34] H. Hurdequint, M. Malouche, FMR studies of Fe bilayers and multilayers $(Ag/Fe)_n$: evidence for a dynamic inter-magnetic layer coupling, J. Magn. Magn. Mater. 93 (1991) 276–280, https://doi.org/10.1016/0304-8853(91)90345-B http://www.sciencedirect.com/science/article/pii/030488539190345B.
[35] H. Wu, C.H. Wan, X. Zhang, Z.H. Yuan, Q.T. Zhang, J.Y. Qin, H.X. Wei, X.F. Han, S. Zhang, Observation of magnon-mediated electric current drag at room temperature, Phys. Rev. B 93 (6) (2016) 060403, https://doi.org/10.1103/PhysRevB.93.060403.
[36] H. Wu, L. Huang, C. Fang, B.S. Yang, C.H. Wan, G.Q. Yu, J.F. Feng, H.X. Wei, X.F. Han, Magnon valve effect between two magnetic insulators, Phys. Rev. Lett. 120 (9) (2018) 097205, https://doi.org/10.1103/PhysRevLett.120.097205 https://link.aps.org/doi/10.1103/PhysRevLett.120.097205.
[37] C.Y. Guo, C.H. Wan, X. Wang, C. Fang, P. Tang, W.J. Kong, M.K. Zhao, L.N. Jiang, B.S. Tao, G.Q. Yu, X.F. Han, Magnon valves based on YIG/NiO/YIG all-insulating magnon junctions, Phys. Rev. B 98 (13) (2018) 134426, https://doi.org/10.1103/PhysRevB.98.134426 https://link.aps.org/doi/10.1103/PhysRevB.98.134426.
[38] J. Wei, J. Wang, Q. Liu, X. Li, D. Cao, X. Sun, An induction method to calculate the complex permeability of soft magnetic films without a reference sample, Rev. Sci. Instrum. 85 (5) (2014) 054705, https://doi.org/10.1063/1.4876598.
[39] A. Vansteenkiste, J. Leliaert, M. Dvornik, M. Helsen, F. Garcia-Sanchez, B. Van Waeyenberge, The design and verification of MuMax3, AIP Adv. 4 (10) (2014) 107133, https://doi.org/10.1063/1.4899186.
[40] V.E. Demidov, M. Evelt, V. Bessonov, S.O. Demokritov, J.L. Prieto, M. Muñoz, J. Ben Youssef, V.V. Naletov, G. de Loubens, O. Klein, M. Collet, P. Bortolotti, V. Cros, A. Anane, Direct observation of dynamic modes excited in a magnetic insulator by pure spin current, Sci. Rep. 6 (1) (2016) 32781, https://doi.org/10.1038/srep32781.
[41] E.N. Beginin, A.V. Sadovnikov, V.K. Sakharov, A.I. Stognij, Y.V. Khivintsev, S.A. Nikitov, Collective and localized modes in 3D magnonic crystals, J. Magn. Magn. Mater. 492 (2019) 165647, https://doi.org/10.1016/j.jmmm.2019.165647 http://www.sciencedirect.com/science/article/pii/S0304885319316178.
[42] O. Mosendz, J.E. Pearson, F.Y. Fradin, S.D. Bader, A. Hoffmann, Suppression of spin-pumping by a MgO tunnel-barrier, Appl. Phys. Lett. 96 (2) (2010) 022502, https://doi.org/10.1063/1.3280378.
[43] L. Mihalceanu, S. Keller, J. Greser, D. Karfaridis, K. Simeonidis, G. Vourlias, T. Kehagias, A. Conca, B. Hillebrands, E.T. Papaioannou, Spin-pumping through a varying-thickness MgO interlayer in Fe/Pt system, Appl. Phys. Lett. 110 (25) (2017) 252406, https://doi.org/10.1063/1.4989678.
[44] E. Padrón-Hernández, A. Azevedo, S.M. Rezende, Amplification of spin waves by thermal spin-transfer torque, Phys. Rev.Lett. 107 (19) (2011) 197203, https://doi.org/10.1103/PhysRevLett.107.197203 https://link.aps.org/doi/10.1103/PhysRevLett.107.197203.
[45] E. Padrón-Hernández, A. Azevedo, S.M. Rezende, Amplification of spin waves in yttrium iron garnet films through the spin Hall effect, Appl. Phys. Lett. 99 (19) (2011) 192511, https://doi.org/10.1063/1.3660586.